Predictions of nuclear charge radii with the radial basis function approach and linear relationship*

Tao Li (李涛)[1,2†] Min Liu (刘敏)[1,2] Ning Wang (王宁)[1,2‡]

[1]Department of Physics,Guangxi Normal University, Guilin 541004, China
[2]Guangxi Key Laboratory of Nuclear Physics and Technology, Guilin 541004, China

Abstract: The linear relationship between the charge radius deviations for nuclei (Z, N) and those for $(Z, N-2)$ is observed in the predictions of the WS* radius formula and HFB25 model. Together with the linear relationship, a modified radial basis function (RBFlr) approach is proposed to further improve the accuracy of the models in charge radius predictions. The root-mean-square deviation with respect to 995 measured nuclear charge radii falls to 0.007 fm, and the charge radii of Ca isotopes can be much better reproduced. In addition, based on the proposed approach, the charge radii of 331 unmeasured nuclei are predicted. This linear correlation combined with RBFlr has the potential to become a typical practice of physically guided machine learning approaches in nuclear physics.

Keywords: nuclear charge radius, radial basis function, linear relationship, WS* radius formula

DOI: 10.1088/1674-1137/ae3e56 **CSTR:** 32044.14.ChinesePhysicsC.50054102

I. INTRODUCTION

The nuclear charge radius, as one of the fundamental properties of the atomic nucleus, is an important physical quantity for characterizing the size of the atomic nucleus. Precise measurements and predictions of nuclear charge radius provide critical insights into structure information of the atomic nucleus, such as isospin [1, 2], shell evolution [3], deformation parameter [4], and exotic halo structure [5]. The information about the symmetry energy of nuclear matter near the saturation density can be obtained based on the difference of the charge radii for the mirror nuclei [2, 6−12]. It is worth noting that the nuclear charge radius is also an important data for testing the accuracy of the standard model [13]. Experimental determination of nuclear charge radius is achieved through multiple precision techniques, including high-energy electron scattering [14, 15], muonic X-ray spectroscopy [16], $K\alpha$ X-ray isotope shift analysis [17], and laser spectroscopic measurements of isotope shifts [18]. With the application of laser spectroscopy technology in the measurement of unstable atomic nuclei, more than 1000 nuclear charge radii have been measured [19−21]. These data have provided strong support for the exploration of nuclear structure and the verification of nuclear theoretical models.

Numerous theoretical methods are used to describe the nuclear charge radius. One type is the semi-empirical formulas proposed based on the $A^{1/3}$ [22] or $Z^{1/3}$ [1] laws, where A and Z represent the mass number and proton number of the atomic nucleus, respectively. As the experimental data accumulate continuously, empirical formulas considering isospin, shell, pairing, and deformation effect corrections have been proposed. The current most accurate empirical formula is the WS* radius formula [2] developed by Wang *et al.*, which incorporates isospin dependence, shell effects, and deformation corrections. In this framework, the shell correction energies and deformation parameters essential for charge radius calculation are derived from the Weizsäcker-Skyrme (WS*) [23] nuclear mass model. Remarkably, the WS* radius formula achieves a root-mean-square (rms) deviation of only 0.022 fm when describing 885 experimental data points, demonstrating exceptional predictive accuracy, and can better describe the kink point caused by the shell effect. Some microscopic methods can also be used to describe the nuclear charge radius, such as the Hartree-Fock-Bogoliubov (HFB) [24−26] model, relativistic mean-field (RMF) [27] model, relativistic continuum Hartree–Bogoliubov (RCHB) [28] model, and covariant density functional theory (CDFT) [29]. The HFB25 [24] model describes the rms deviation of 884 experimental data as

Received 15 December 2025; Accepted 26 January 2026; Accepted manuscript online 27 January 2026

* Supported by the Guangxi "Bagui Scholar" Teams for Innovation and Research Project, the Natural Science Foundation of Guangxi (2025JJA110131), the National Natural Science Foundation of China (12265006, 12375129, U1867212), the Central Government Guidance Funds for Local Scientific and Technological Development, China (Guike ZY22096024), and the Guangxi Normal University National Natural Science Foundation joint cultivation project (2024PY010)

† E-mail: litao@gxnu.edu.cn

‡ E-mail: wangning@gxnu.edu.cn

©2026 Chinese Physical Society and the Institute of High Energy Physics of the Chinese Academy of Sciences and the Institute of Modern Physics of the Chinese Academy of Sciences and IOP Publishing Ltd. All rights, including for text and data mining, AI training, and similar technologies, are reserved.

0.025 fm. The CDFT can better describe the odd-even effect of nuclear charge radius. In addition, some local relations can effectively predict the nuclear charge radius, such as the Garvey-Kelson (GK) relations [30] and charge radius relations of neighboring nuclei [31, 32]. Recently, an interesting linear correlation of deviation between theoretical predictions and experimental databases for nuclear charge radii was observed, and the accuracy of the theoretical model in describing the nuclear charge radius can be improved by this linear correlation [33].

Machine learning techniques have demonstrated remarkable efficacy across diverse nuclear physics applications, such as nuclear mass prediction [34−52], fission yield estimation [53, 54], nuclear decay half-life prediction [55−57], and symmetry energy slope parameter extraction [58−60]. These applications highlight the transformative potential of data-driven approaches in addressing complex nuclear phenomena. To further enhance the accuracy of the theoretical model in describing the nuclear charge radius, the radial basis function (RBF) [21], Bayesian neural network (BNN) [61−63], kernel ridge regression (KRR) [64, 65], and other machine learning approaches [66, 67] have been introduced. These machine learning approaches are essentially based on training the residuals between the theoretical model predictions and experimental values to further improve the prediction accuracy of nuclear charge radii. This traditional method of training residuals has now reached a bottleneck, even when multiple machine learning algorithms are employed. Therefore, it is extremely urgent to explore new physical mechanisms to further enhance the reliability of the machine learning approach in predicting the nuclear charge radius.

In this work, a linear relationship was combined with the RBF approach to predict the nuclear charge radii (for nuclei with $Z \geq 8$, $N \geq 8$). The methodological details of the RBF approach combined with the linear relationship are presented in Section II. Section III provides the results and discussion, and the main conclusions are summarized in Section IV.

II. NUMERICAL DETAILS

The conventional method for predicting nuclear charge radius using the RBF approach involves training on experimental and theoretical deviations $\Delta R_{\rm c}(Z,N) = R_{\rm c}^{\rm exp}(Z,N) - R_{\rm c}^{\rm th}(Z,N)$ to reconstruct the function $S(Z,N)$. The revised charge radius of nucleus (Z,N) is given by

$$R_{\rm c}^{\rm RBF}(Z,N) = R_{\rm c}^{\rm th}(Z,N) + S(Z,N). \tag{1}$$

To address the systematic deviations inherent in conventional theoretical predictions and experimental measurements, we conducted a comprehensive analysis of the relationship between nuclear charge radius deviations $\Delta R_{\rm c}(Z,N)$ and $\Delta R_{\rm c}(Z,N-2)$. The WS* radius formula [2] and HFB25 model are used for the calculations of charge radii $R_{\rm c}^{\rm th}$. Figure 1 demonstrates a strong linear relationship between nuclear charge radius deviations $\Delta R_{\rm c}(Z,N)$ and $\Delta R_{\rm c}(Z,N-2)$, with a Pearson linear correlation coefficient reaching 0.8. This linear relationship may reflect the influence of the isospin effect on the nuclear charge radius. It is possible to achieve a fusion of the physical mechanism and data-driven approach by combining this linear relationship with the RBF approach. The RBF approach considering linear relationship (RBFlr) trains residual $\delta(Z,N) = \Delta R_{\rm c}(Z,N) - \Delta R_{\rm c}(Z,N-2)$ to obtain the new reconstruction function, $S^{\rm lr}(Z,N)$. The revised charge radius of neutron-rich nucleus (Z,N) is then given by

$$R_{\rm c}^{\rm RBFlr}(Z,N) = R_{\rm c}^{\rm th}(Z,N) + \Delta R_{\rm c}(Z,N-2) + S^{\rm lr}(Z,N). \tag{2}$$

Similarly, the revised charge radius of proton-rich nucleus $(Z,N-2)$ is given by

$$R_{\rm c}^{\rm RBFlr}(Z,N-2) = R_{\rm c}^{\rm th}(Z,N-2) + \Delta R_{\rm c}(Z,N) - S^{\rm lr}(Z,N). \tag{3}$$

The calculation details for $S^{\rm lr}(Z,N)$ are similar to those of the traditional RBF approach and can be found in the Refs. [21, 34−36]. For convenience, the theoretical model improved wth the RBFlr approach is denoted by "model+RBFlr". To evaluate the predictive power of model+RBFlr, the rms deviation

$$\sigma = \sqrt{\frac{1}{n}\sum_{i=1}^{n}(R_{\rm c}^{\rm exp} - R_{\rm c}^{\rm th})^2}, \tag{4}$$

is employed, where $R_{\rm c}^{\rm exp}$ and $R_{\rm c}^{\rm th}$ are the experimental and theoretical nuclear charge radii, respectively, and n is the number of nuclei contained in a given set.

III. RESULTS AND DISCUSSION

To evaluate the predictive power of the RBFlr approach, the measured 1028 charge radii [19−21] for nuclei ($Z \geq 8$, $N \geq 8$) are used in the analysis. We selected 855 atomic nucleus pairs based on the new training data approach. First, the charge radii of 855 neutron-rich nuclei are predicted based on Eq. (2) using the leave-one-out cross-validation method and compared with the prediction results of the model and the model combined with the RBF approach. Figure 2 shows the trend of the deviations between the theoretical and experimental charge

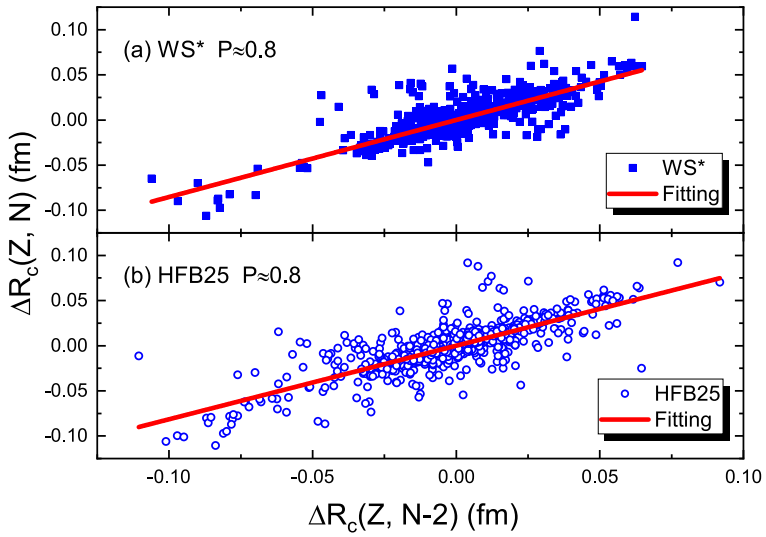

Fig. 1. (color online) Relationship between $\Delta R_c(Z,N)$ and $\Delta R_c(Z,N-2)$. The squares and circles denote the results of the WS* radius formula and HFB25 model, respectively.

radii of 855 neutron-rich nuclei as a function of the neutron number. As demonstrated in Fig. 2(a), the RBFlr approach exhibits significant advantages over the conventional RBF approach in enhancing the prediction accuracy of the WS* radius formula. While the traditional RBF approach reduced the rms deviation of prediction results for WS* radius formula from 0.021 to 0.016 fm (a 23.8% improvement), the RBFlr approach achieved substantially greater enhancement, decreasing the rms deviation from 0.021 to 0.008 fm, corresponding to a 61.9% improvement. Similarly, the RBFlr approach also played a significant role in improving the prediction results of the HFB25 model. As shown in Fig. 2(b), when the HFB25 model is combined with the RBFlr approach, the rms deviation of the charge radii of 855 nuclei decreases from 0.025 to 0.013 fm, improving by 48.0%. However, when the HFB25 model is combined with the RBF approach, the rms deviation of the nuclear charge radius can only be reduced to 0.018 fm, improving by only 28.0%. This comparative analysis demonstrates that the RBFlr approach exhibits superior performance in enhancing the predictive accuracy of theoretical models for nuclear charge radii when compared to the conventional RBF approach. This advantage of the RBFlr approach is even more evident around neutron number $N = 90$, as shown in Fig. 2. Based on a systematic analysis of experimental data on nuclear charge radii, we found that theoretical models show systematic deviations in describing the nuc-

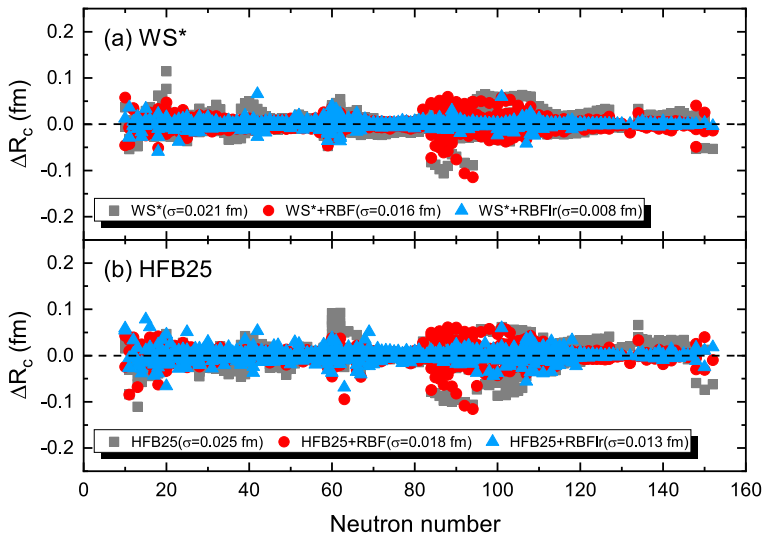

Fig. 2. (color online) Trend of the deviations between the theoretical and experimental charge radii of 855 neutron-rich nuclei as a function of the neutron number. (a) The squares, dots, and triangles respectively represent the prediction results of the WS* radius formula and its combination with the RBF and RBFlr approaches. (b) Same as (a) but for the HFB25 model.

lear charge radii of this nuclei region. The atomic nuclei in this region may possess a non-axisymmetric tetrahedral structure [68], which could lead to anomalous charge radii. The systematic deviations in describing the charge radii of nuclei in this region provided by the WS* radius formula and HFB25 model may arise from the fact that only axisymmetric quadrupole and hexadecapole deformations were accounted for in the calculations. Because the RBFlr approach requires the introduction of the deviation of the adjacent nuclear charge radius as one of the correction terms, it can counteract this kind of systematic deviation. However, this systematic deviation compensation does not apply to the description of the nucleus with the first abnormal increase in charge radius along the isotope chain, such as ^{181}Hg. Therefore, in Fig. 2, we can observe that in the results improved by the RBFlr approach, there are a few points with larger deviations. The probability of similar risks occurring in the region of lighter atomic nuclei is also higher because of the presence of exotic structures. It is worth noting that the prediction of the charge radii for proton-rich nuclei based on Eq. (3) also shows the same degree of improvement.

To systematically evaluate the extrapolation capability of the RBFlr approach, we constructed two distinct test sets: test set 01 specifically targeting neutron-rich nuclei and test set 02 focusing on proton-rich nuclei. The corresponding learning sets for both test sets were carefully selected from the comprehensive dataset of 855 nuclei pairs mentioned above. For test set 01, 117 nuclei were selected from a pool of 855 atomic nuclei (Z, N) (with proton number Z and neutron number N), ensuring these selected nuclei were absent from the corresponding 855 atomic nuclei $(Z, N-2)$ dataset. Test set 01 is paired with learning set 01, which comprises 715 nuclei extracted from the 855 atomic nuclei $(Z, N-2)$ dataset. Similarly, for test set 02, 117 nuclei were chosen from the 855 atomic nuclei $(Z, N-2)$ dataset, with their counterparts in the 855 atomic nuclei (Z, N) dataset intentionally excluded. Test set 02 corresponds to learning set 02, which includes 715 nuclei sampled from the 855 atomic nuclei (Z, N) dataset. The spatial distribution and composition characteristics of these learning and test sets are visually presented in Fig. 3. Figure 3 reveals that a significant proportion of atomic nuclei in test sets 01 and 02 reside outside the spatial distribution of their respective learning sets. Consequently, the charge radius predictions for these nuclei inherently involve extrapolation beyond the established learning domains. Figure 4 shows the trend of the deviations between the theoretical and experimental charge radii of test sets 01 and 02 as a function of the proton number. As can be seen from Fig. 4(a), for test set 01, the rms deviation between the prediction results of the WS* radius formula and experimental values is 0.027 fm. The WS* radius formula combined with the RBF approach showed an rms deviation of test set 01 of 0.019 fm, which is a 29.6% improvement. The WS* radius formula combined with the RBFlr approach showed an rms deviation of test set 01 of 0.015 fm, which is a 44.4% improvement. As can be seen from Fig. 4(b), for test set 02, the improvement in the prediction results of the WS* radius formula by the RBFlr approach is greater than that of the RBF approach. When the WS* radius formula is combined with the RBFlr approach, the rms deviation in describing the nuclear charge radii of test set 02 reaches 0.016 fm. It is worth noting that the WS* radius formula combined with the RBFlr approach yields slightly better extrapolation results for the neutron-rich region compared to those for the proton-rich region. We speculate

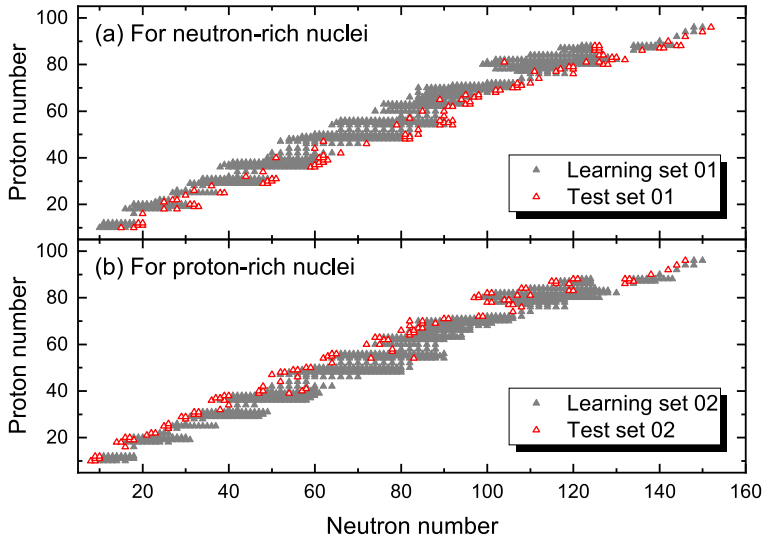

Fig. 3. (color online) Distributions of learning and test sets. (a) The solid and hollow triangles respectively represent learning set 01 and test set 01, where test set 01 is mainly located in the neutron-rich region. (b) The solid and the hollow triangles respectively represent learning set 02 and test set 02, where test set 02 is mainly located in the proton-rich region.

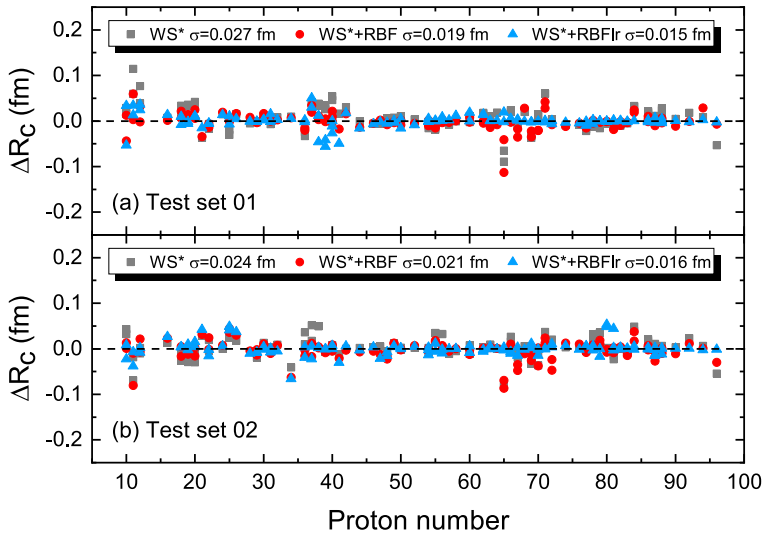

Fig. 4. (color online) Trend of the deviations between the theoretical and experimental charge radii of test sets 01 and 02 as a function of proton number. (a) The squares, dots, and triangles respectively represent the prediction results of the WS* radius formula and its combination with the RBF and RBFlr approaches for test set 01. (b) Same as (a) but for test set 02.

that, in the proton-rich region, the Coulomb interaction may have disrupted the isospin symmetry, thereby reducing the accuracy in describing the nuclear charge radius. Furthermore, as can be seen in Fig. 4, a similar phenomenon is observed to that in Fig. 2. In the region of proton number $Z = 65 - 71$, the deviation of the WS* radius formula prediction results is significantly improved by the RBFlr approach, while in the region around proton numbers $Z = 40$ and 80, a few data actually increased. The reason for this similar phenomenon is also the abnormal increase in charge radius due to the deformation evolution of the atomic nucleus. The computational results reveal that the HFB25 model integrated with the RBFlr approach exhibits prediction patterns analogous to those of the WS* radius formula for test sets 01 and 02, but the latter achieves superior accuracy. It is worth noting that the WS* radius formula combined with the RBFlr approach can describe the nuclear charge radii of test sets 01 and 02 with rms deviations that are comparable to the errors of a portion of the experimental data for nuclear charge radii. Although the extrapolation range of this method is relatively limited, based on existing experimental data, we can provide charge radii for 1326 nuclei based on the WS* radius formula combined with the RBFlr approach, where the charge radii for 331 nuclei are not measured experimentally. Moreover, the rms deviation between the predicted and experimental values of the charge radii for the remaining 995 nuclei is only 0.007 fm.

The accurate prediction of charge radii in the Ca isotope chain presents a persistent challenge for theoretical models, primarily due to two competing effects: the abrupt structural transitions associated with magic numbers and the characteristic odd-even staggering phenomena. To further test the predictive ability of the RBFlr approach, in Fig. 5 (a) we present the experimental values of the charge radius of the Ca isotope chain, as well as the predicted values of the WS* radius formula and its combination with the RBFlr approach. Figure 5(a) demonstrates that while the WS* radius formula successfully captures the overall trend of charge radius evolution in the Ca isotope chain, including the characteristic inflection point at neutron magic number $N = 28$, it exhibits notable limitations in reproducing the odd-even staggering phenomenon. Notably, the WS* radius formula combine RBFlr approach hybrid configuration shows significantly improved agreement with experimental odd-even patterns. Figure 5(a) particularly highlights the cases of ^{53}Ca and ^{54}Ca, where the WS* radius formula predict a pronounced inflection point at $N = 32$. However, this artificial feature is conspicuously absent in the WS* radius formula combine RBFlr approach predictions, suggesting that the latter method provides a more physically realistic description of nuclear charge radii evolution in this region based on the trend of charge radii for the K isotope chain [3]. Figure 5(b) demonstrates the variation of the charge radii along the Pb isotope chain as a function of neutron number. The inflection point phenomenon, which is attributed to neutron magic number $N = 126$, is successfully captured by both the WS* radius formula and its combined RBFlr approach. However, the predictions derived from the integration of the WS* radius formula with the RBFlr approach exhibit superior agreement with the experimental data for the Pb isotope chain.

IV. SUMMARY

The deviations between the predicted and experiment-

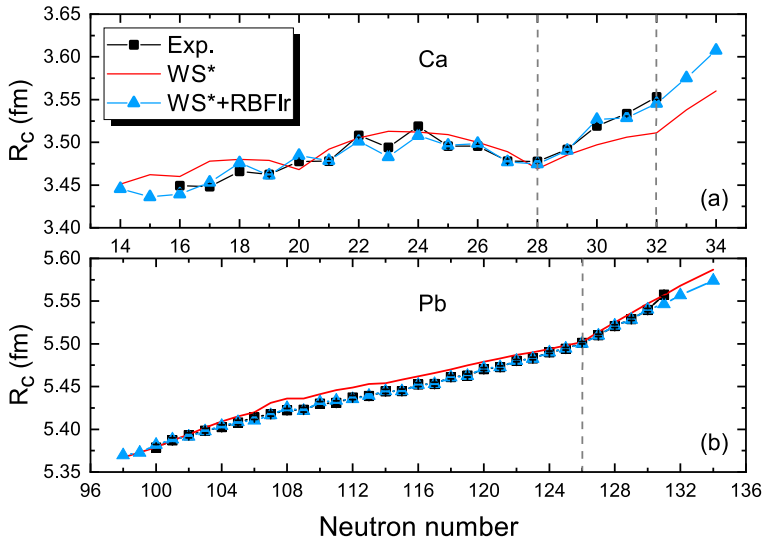

Fig. 5. (color online) Trend of charge radii of the Ca and Pb isotope chains with neutron number. Squares represent the experimental values, and vertical lines represent error bars. The solid lines and triangles represent the prediction results of the WS* radius formula and its combination with the RBFlr approach, respectively.

al values of nuclear charge radii were systematically analyzed based on the WS* radius formula and HFB25 model. The linear relationship of the charge radius deviations between nuclei (Z, N) and $(Z, N-2)$ was found. The RBFlr approach, which combines an RBF approach with a linear relationship, was proposed to enhance the predictive accuracy of nuclear charge radii. The RBFlr approach exhibited significant advantages over the conventional RBF approach in enhancing the prediction accuracy of the WS* radius formula and HFB25 model. The integration of the WS* radius formula with the RBFlr approach demonstrated remarkable predictive performance, achieved an rms deviation of merely 0.008 fm between theoretical predictions and experimental measurements for 855 atomic nuclei. The prediction accuracy of the new results was 61.9% higher than that of the WS* radius formula's predictions. Similarly, the HFB25 model combined with the RBFlr approach showed an rms deviation of the charge radii of 855 nuclei decreasing from 0.025 fm to 0.013 fm, improving by 48.0%.

For the extrapolation prediction of nuclear charge radii, the RBFlr approach also has significant advantages over the RBF approach. The rms deviation for extrapolating the charge radii of nuclei in the neutron-rich region with the WS* radius formula combined with the RBFlr approach can reach 0.015 fm. The charge radii for 1326 nuclei were predicted based on the WS* radius formula combined with the RBFlr approach, including 331 nuclei for which experimental data are currently unavailable. For the remaining 995 nuclei with available experimental measurements, the WS* radius formula combined with the RBFlr approach achieved an exceptional rms deviation of merely 0.007 fm, and the charge radii of the calcium isotope chain were well described.

This linear relationship transcends mere empirical regularity, it may have captured the collective or higher-order term effects of isospin on the nuclear charge radius, which goes beyond the simple isospin correction term already present in the WS* radius formula. By combining this relationship with machine learning approaches, it is possible to achieve a fusion of physical mechanisms and data-driven approaches, which could potentially become a typical practice of guiding machine learning approaches by physics in nuclear physics.

DATA AVAILABILITY STATEMENT

The nuclear charge radius tables with the WS radius formula combined with RBFlr approach are available from www.imqmd.com/mass/Rch_RBFlr.txt.*

References

[1] S. Q. Zhang, J. Meng, S. G. Zhou *et al.*, Eur. Phys. J. A **13**, 285 (2002)

[2] N. Wang and T. Li, Phys. Rev. C **88**, 011301(R) (2013)

[3] Á. ZKoszorús, X. F. Yang, W. G. Jiang *et al.*, Nat. Phys. **17**, 439 (2021)

[4] B. A. Marsh, T. Day Goodacre, S. Sels *et al.*, Nat. Phys. **14**, 1163 (2018)

[5] W. Nörtershäuser, D. Tiedemann, M. Žáková *et al.*, Phys. Rev. Lett **102**, 062503 (2009)

[6] B. A. Brown, Phys. Rev. Lett **119**, 122502 (2017)

[7] B. A. Brown, K. Minamisono, J. Piekarewicz *et al.*, Phys. Rev. Res. **2**, 022035(R) (2020)

[8] S. V. Pineda, K. König, D.M. Rossi *et al*., Phys. Rev. Lett. **127**, 182503 (2021)
[9] Y. N. Huang, Z. Z. Li, and Y. F. Niu, Phys. Rev. C **107**, 034319 (2023)
[10] P. Bano, S. P. Pattnaik, M. Centelles *et al*., Phys. Rev. C **108**, 015802 (2023)
[11] S. Gautam, A. Venneti, S. Banik *et al*., Nucl. Phys. A **1043**, 122832 (2024)
[12] X. R. Ma, S. Sun, R. An *et al*., Chin. Phys. C **48**, 084104 (2024)
[13] C. Y. Seng, Phys. Rev. Lett. **130**, 152501 (2023)
[14] I. Sick, Prog. Part. Nucl. Phys. **47**, 245 (2001)
[15] K. Tsukada, Y. Abe, A. Enokizono *et al*., Phys. Rev. Lett. **131**, 092502 (2023)
[16] T. Y. Saito, M. Niikura, T. Matsuzaki *et al*., Phys. Rev. C **111**, 034313 (2025)
[17] G. Fricke, C. Bernhardt, K. Heilig *et al*., At. Data Nucl. Data Tables **60**, 177 (1995)
[18] S. W. Bai, X. F. Yang, Á. Koszorús *et al*., Phys. Rev. Lett. **134**, 182501 (2025)
[19] I. Angeli and K. P. Marinova, At. Data Nucl. Data Tables **99**, 69 (2013)
[20] T. Li, Y. Luo, and N. Wang, At. Data Nucl. Data Tables **140**, 101440 (2021)
[21] T. Li, H. Yao, M. Liu *et al*., Nucl. Phys. Rev. **40**, 31 (2023)
[22] Z. Sheng, G. Fan, J. Qian *et al*., Eur. Phys. J. A **51**, 40 (2015)
[23] N. Wang, Z. Liang, M. Liu *et al*., Phys. Rev. C **82**, 044304 (2010)
[24] S. Goriely, N. Chamel, and J. M. Pearson, Phys. Rev. C **88**, 024308 (2013)
[25] S. Goriely, N. Chamel, and J. M. Pearson, Phys. Rev. C **88**, 061302(R) (2013)
[26] S. Goriely, N. Chamel, and J. M. Pearson, Phys. Rev. C **93**, 034337 (2016)
[27] L. Geng, H. Toki, and J. Meng, Prog. Theor. Phys. **113**, 785 (2005)
[28] X. W. Xia, Y. Lim, P. W. Zhao *et al*., At. Data Nucl. Data Tables **121-122**, 1 (2018)
[29] R. An, X. Jiang, N. Tang *et al*., Chin. Phys. C **49**, 064105 (2025)
[30] J. Piekarewicz, M. Centelles, X. Roca-Maza *et al*., Eur. Phys. J. A **46**, 379 (2010)
[31] B. H. Sun, Y. Lu, J. P. Peng *et al*., Phys. Rev. C **90**, 054318 (2014)
[32] M. Bao, Y. Lu, Y. M. Zhao *et al*., Phys. Rev. C **94**, 064315 (2016)
[33] R. Shou, X. Yin, C. Ma *et al*., Phys. Rev. C **106**, L061304 (2022)
[34] N. Wang and M. Liu, Phys. Rev. C **84**, 051303(R) (2011)
[35] Z. M. Niu, Z. L. Zhu, Y. F. Niu *et al*., Phys. Rev. C **88**, 024325 (2013)
[36] Z. M. Niu, B. H. Sun, H. Z. Liang *et al*., Phys. Rev. C **94**, 054315 (2016)
[37] Z. M. Niu and H. Z. Liang, Phys. Lett. B **778**, 48 (2018)
[38] Y. Liu, C. Su, J. Liu *et al*., Phys. Rev. C **104**, 014315 (2021)
[39] J. Xie, K. Wang, C. Wang *et al*., Phys. Rev. C **109**, 064317 (2024)
[40] X. H. Wu and P. W. Zhao, Phys. Rev. C **101**, 051301(R) (2020)
[41] X. H. Wu, L. H. Guo, and P. W. Zhao, Phys. Lett. B **819**, 136387 (2021)
[42] X. H. Wu, Y. Y. Lu, and P. W. Zhao, Phys. Lett. B **834**, 137394 (2022)
[43] X. H. Wu, Front. Phys. **11**, 1061042 (2023)
[44] X. H. Wu, C. Pan, K. Y. Zhang *et al*., Phys. Rev. C **109**, 024310 (2024)
[45] X. H. Wu and C. Pan, Phys. Rev. C **110**, 034322 (2024)
[46] X. Y. Zhang, H. R. Liu, L. L. Liu *et al*., Phys. Rev. C **110**, 044307 (2024)
[47] Y. Y. Guo, T. Yu, X. H. Wu *et al*., Phys. Rev. C **110**, 064310 (2024)
[48] Y. Lu, T. Shang, P. Du *et al*., Phys. Rev. C **111**, 014325 (2025)
[49] H. Liu, J. Lei, and Z. Ren, Phys. Rev. C **111**, 024316 (2025)
[50] W. Ye and N. Wan, Phys. Rev. C **111**, 044317 (2025)
[51] I. Bentley, J. Tedder, M. Gebran *et al*., Phys. Rev. C **112**, 014324 (2025)
[52] A. Jalili, F. Pan, A. X. Chen *et al*., Phys. Rev. C **112**, 024305 (2025)
[53] Z. A. Wang, J. Pei, Y. Liu *et al*., Phys. Rev. Lett. **123**, 122501 (2019)
[54] C. Y. Qiao, J. C. Pei, Z. A. Wang *et al*., Phys. Rev. C **103**, 034621 (2021)
[55] N. N. Ma, X. J. Bao, and H. F. Zhang, Chin. Phys. C **45**, 024105 (2021)
[56] N. N. Ma, T. L. Zhao, W. X. Wang *et al*., Phys. Rev. C **107**, 014310 (2023)
[57] H. Q. You, X. T. He, R. H. Wu *et al*., Nucl. Sci. Tech. **36**, 191 (2025)
[58] J. Xu, W. J. Xie, and B. A. Li, Phys. Rev. C **102**, 044316 (2020)
[59] J. Xu, Chin. Phys. Lett. **38**, 042101 (2021)
[60] Y. Wang, Z. Gao, H. Lü *et al*., Phys. Lett. B **835**, 137508 (2022)
[61] X. X. Dong, R. An, J. X. Lu *et al*., Phys. Lett. B **838**, 137726 (2023)
[62] X. Zhang, H. He, G. Qu *et al*., Phys. Rev. C **110**, 014316 (2024)
[63] J. Liu, K. Z. Tan, L. Wang *et al*., Nucl. Sci. Tech. **36**, 215 (2025)
[64] J. Q. Ma and Z. H. Zhang, Chin. Phys. C **46**, 074105 (2022)
[65] L. Tang and Z. H. Zhang, Nucl. Sci. Tech. **35**, 19 (2024)
[66] Y. Y. Cao, J. Y. Guo, and B. Zhou, Nucl. Sci. Tech. **34**, 152 (2023)
[67] T. S. Shang, H. H. Xie, J. Li *et al*., Phys. Rev. C **110**, 014308 (2024)
[68] K. Mazurek, J. Dudek, A. Góźdź *et al*., Acta Phys. Pol. B **40**, 731 (2009)